Cyclic Trinuclear Copper(I), Silver(I), and Gold(I) Complexes: A Theoretical Insight.

Journal:	*Dalton Transactions*
Manuscript ID:	DT-ART-08-2014-002514.R1
Article Type:	Paper
Date Submitted by the Author:	30-Sep-2014
Complete List of Authors:	Caramori, Giovanni; Universidade Federal de Santa Catarina, Departamento de Química Piccoli, Rafael; Universidade Federal de Santa Catarina, Departamento de Química Segala, Maximiliano; Universidade Federal do Rio Grande do Sul, Instituto de Quimica Muñoz-Castro, Alvaro; Universidad Autonoma de Chile, Direccion de Postgrado e Investigacion Guajardo-Maturana, Raul; Universidad Andres Bello, Departamento de Ciencias Química Andrada, Diego; Philipps-Universität Marburg, Fachbereich Chemie Frenking, G; Philipps-Universitat Marburg, Fachbereich Chemie

Analysis of the bonding and magnetic response in Ligand supported coinage metal macrocycles

Cyclic Trinuclear Copper(I), Silver(I), and Gold(I) Complexes: A Theoretical Insight.[†]

Giovanni F. Caramori,[*a,e] **Rafael M. Piccoli,**[a] **Maximiliano Segala,**[b] **Alvaro Muñoz-Castro,**[c] **Raul Guajardo-Maturana,**[d] **Diego M. Andrada,**[e] **and Gernot Frenking**[e]

Received Xth XXXXXXXXXX 20XX, Accepted Xth XXXXXXXXX 20XX
First published on the web Xth XXXXXXXXXX 200X
DOI: 10.1039/b000000x

The metal-ligand, M−L, bonding situation in cyclic trinuclear complexes, CTCs, of copper(I), silver(I), and gold(I) was investigated at the light of the energy decomposition analysis (EDA-NOCV) and natural bond orbitals (NBO). The anisotropy of the induced current density (ACID) and magnetic response were employed to evaluate the effect of electronic conjugation and metal-metal interactions in CTCs. The EDA-NOCV results show that the M−L bonding is stronger in gold(I) than in copper(I) or silver(I) complexes. Au$^+$−L bonds present an elevated covalent character when compared with Cu$^+$−L and Ag$^+$−L bonds. The NBO analysis confirms the elevated covalent character observed for Au$^+$−L bonds, indicating that the ligand-metal donation, L→M, and the metal-ligand back-donation, M→L, are more stabilizing in gold(I) than in copper(I) or silver(I) complexes. Both ACID and the magnetic response calculations reveal that there is cyclic conjugations in the ligands and a strong diatropic ring current indicating the presence of aromaticity. However, there is no *through-bond* M−L conjugation between the ligands and the metallic centers, as indicated by the absence of a continuous anisotropy boundary surface involving M−L bonds.

1 Introduction

Triangular arrangements of coinage metal ions such Cu$^+$([Ar]3d^{10}), Ag$^+$([Kr]4d^{10}), and Au$^+$([Xe]4f^{14}5d^{10}) are common in chemistry, specially due to their luminescent properties and ability to form supramolecular structures.[1–16] Vaughan and coworkers[17] have synthesized the first gold(I) cyclic trinuclear complex (CTC) [Au(I)$_3$(μ-1,2-piridyl)$_3$], which presents a planar 9-membered ring structure, exhibiting a roughly D_{3h} symmetry.

The synthesis of CTCs such as [M$_3$(μ-L)$_3$] (where M = Cu$^+$, Ag$^+$, Au$^+$ and L = pyrazolate (pz), imidazolate, triazolates, pyridiniate and others), their aggregates,[3] and consequently their physical properties are intimately related to metal-metal and metal-ligand interactions, which are dependent on correlation and relativistic effects, as observed by going from top to bottom in XI group.[18] The presence of aurophilic interactions in CTCs containing gold becomes clear when aggregates of stable mixed-valence Au$_2^{(I)}$([Xe]4f^{14}5d^{10}) / Au$^{(III)}$([xe]4f^{14}5d^8) metallocycles are formed, confirming the presence of an extended electronic structure among the interacting gold atoms.[19] The general tendency to form aggregates supporting d^{10}−d^{10} closed-shell interactions[18,20] has been attributed to electronic correlation, being reinforced by relativistic effects, particularly relevant for gold counterparts. Usually, d^{10}−d^{10} contacts exhibit distances shorter than the sum of the van der Waals radii of the involved centers, resulting in a situation which has been coined as metallophilic interaction. In this respect, the ligand to metal donation results in the population of the ns-based levels of the closed-shell core, which has been described as a useful characteristic to denote both short or long d^{10}−d^{10} contacts,[21–23] where in the former case the bonding combinations are mainly populated leading to distances sizably shorter than the sum of the van der Waals radii, contributing to the metallophilic situation. The most common bridging ligands employed in CTCs are the anionic heterocycles of five members[24] such as pyrazolate, triazolate, imidazolate, and their substituted derivatives. Heterocyclic compounds having six-member rings, such as pyridiniate,[17] and open chain ligands, such as bidentated carbeniates[3,25] are also employed. CTCs containing gold(I) and pyrazolate ligands are employed in the preparation of luminescent materials.[26,27] Cano and coworkers have shown that CTCs such [Au(I)$_3$(μ-pzR(n))$_3$] and [Au(I)$_3$(μ-HpzR(n))$_3$]

[†] Electronic Supplementary Information (ESI) available: [details of any supplementary information available should be included here]. See DOI: 10.1039/b000000x/

[a] *Departamento de Química, Universidade Federal de Santa Catarina, CP 476, Florianópolis, SC, 88040-900, Brazil. Fax: +55 48 3721-6852; Tel: +55 48 3721-6839; E-mail: giovanni.caramori@ufsc.br*
[b] *Instituto de Química, Universidade Federal do Rio Grande do Sul, UFRGS, Porto Alegre, RS, Brazil.*
[c] *Direccion de Postgrado e Investigacion, Sede Providencia, Universidad Autonoma de Chile, Carlos Antunez 1920, Santiago, Chile.*
[d] *Departamento de Ciências Químicas, Universidad Andres Bello, Republica 275, Santiago, Chile*
[e] *Fachbereich Chemie - Philipps-Universität Marburg, Hans-Meerwein-Strasse, D-35032, Marburg, Germany*

(R(n) = $C_6H_4OC_nH_{2n+1}$) exhibit luminescence, which has a stringent dependency on the nature of the ligand instead of the presence of Au(I)-Au(I) interactions. The authors attributed the origin of the luminescence to both ligand-to-metal charge transfer (LMCT) and ligand-to-metal-metal charge transfer (LMMCT).[26]

It has also been shown that CTCs containing the same ligands but with different metal ions such as Cu^+, Ag^+, or Au^+ differs not only in their structural parameters, but also in the electronic structure.[28] Flacker and coworkers have synthesized and determined the crystallographic structures of complexes like $[Au_3(\mu\text{-3,5-Ph}_2pz)_3]$, $[Ag_3(\mu\text{-3,5-Ph}_2pz)_3]$, and $[Cu_3(\mu\text{-3,5-Ph}_2pz)_3]$,[29,30] showing that the gold complex exhibits a planar structure, while silver and copper complexes show significant deviation from planarity as well as the metal-ligand bond lengths are different, Au-N are slightly shorter than Ag-N and Cu-N. Another important feature of CTCs is the amplified π-acidity and π-basicity that they present.[1–3,6,12–15] The π-acid/base properties are responsible for the formation of the supramolecular extended stacks with arenes.[9] Tekarli et al.[12] have shown that CTCs like $[M_3(\mu\text{-L})_3]$ where M = Cu^+, Ag^+, or Au^+ and L = carbeniate, pyrazolate, imidazolate, triazolate, and pyridiniate, show enhanced π-acidity and π-basicity in comparison with their organic counterparts. The π-acidity and π-basicity can be finely tuned according to the nature of the bridging ligand, L, employed. Recently, Titov[31] has shown that the interaction of substituted acylferrocenes macrocycles $[M_3(\mu\text{-L})_3]$ (where M = Cu^+ and Ag^+; L = 3,5-bis(trifluoromethyl)pyrazolate) occurs through the coordination of the CO and phenyl groups with the three metal atoms of the macrocycle. However, interactions between the π-system of the ferrocarbonyl fragments and the macrocycles are absent. The previous theoretical and experimental studies showed that in CTCs there is a direct interplay between the nature of the metal and ligands employed and the strength of metal-ligand and metal-metal interactions. This article reports a comprehensive computational study, in which the nature of the metal-ligand bond, M-L, and the electronic structure of CTCs like $[M_3(\mu\text{-L})_3]$ (where M = Cu^+, Ag^+, and Au^+ and L = pyrazolate with or without substituents R (**1a**-**1c**; **7c**, **8c**) , μ-1,2-isoxazole (**2a**-**2c**), μ-2-pyridyl (**3a**-**3c**), μ-pyridazine (**4a**-**4c**), μ-2-pyrimidyl (**5a**-**5c**), and μ-2-pyrazinil (**6a**-**6c**) are investigated (Figure 1). The choice of such ligands is based on the fact that the literature provides a plentiful supply of studies employing CTCs containing pyrazolate, while studies of CTCs having other bridging ligands such as μ-1,2-isoxazole, μ-2-pyridyl, μ-pyridazine, μ-2-pyrimidyl, μ-2-pyrazinil, and others are scarce. For that reason, the present study investigate the nature of metal-bonding interactions in CTCs and their dependence on the nature of ligands and coinage metals employed, providing therefore valuable information to the rational design of CTCs with tunable properties. In order to shed light on the M-L bonding situation, the EDA-NOCV scheme[32] is employed. The EDA-NOCV scheme decomposes the interaction energy into terms such as electrostatic, pauli repulsion, orbital, and dispersion. The effect of electronic conjugation and metal-metal interactions in CTCs is evaluated through NBO,[33,34] ACID[35,36] and magnetic response[37,38] analyses.

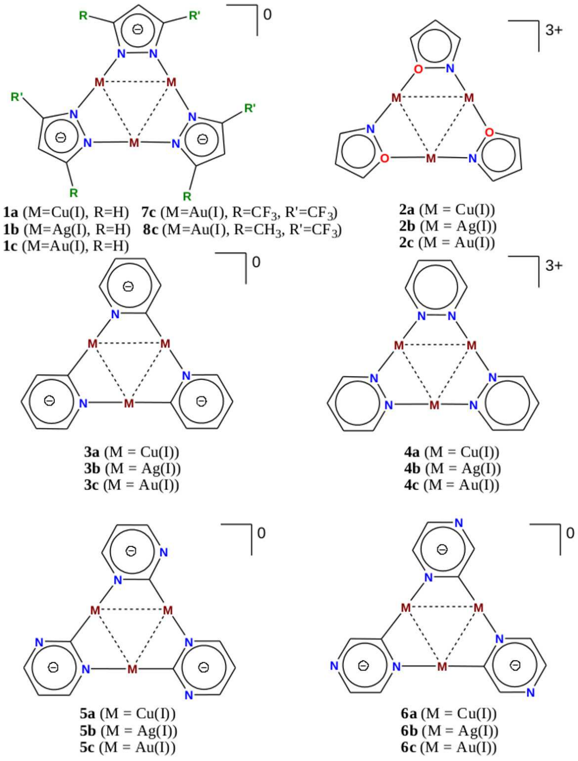

Fig. 1 Schematic representation of the CTCs.

2 Computational Methods

The geometries of complexes **1a**-**8c** (Figure S1, supporting information) were optimized without constraints at the non-local DFT level of theory,[39,40] by using the BP86 functional[41,42] in conjunction with the atom pairwise dispersion correction,[43–45] BP86-D3, and the Ahlrichs triple-ζ-quality basis set, def2-TZVP.[46] Scalar relativistic effects were computed with the zero-order regular approximation, ZORA.[47] All geometry optimizations were performed employing the ORCA package.[48] The model BP86-D3/def2-TZVP has provided data in excellent agreement with the available x-ray structures (Figure S1).[3,19,25,27,28] All reported structures, **1a**-**8c**, were characterized as minimum on the potential energy surfaces by the absence of imaginary eigenvalues in the Hessian matrix. The metal-ligand bonding situation in CTCs **1a-8c** $M_3(\mu\text{-L})_2^{q/q+1}$, where M = Au$^+$, Ag$^+$, Cu$^+$ and L = pyrazolate with or without substituents R (**1a-1c**; **7c**, **8c**), μ-1,2-isoxazole (**2a-2c**), μ-2-pyridyl (**3a-3c**), μ-pyridazine (**4a-4c**), μ-2-pyrimidyl (**5a-5c**), and μ-2-pyrazinil (**6a-6c**) was characterized through the EDA-NOCV[32] approach by employing the Becke-Perdew exchange-correlation functional with an inclusion of the dispersion correction (BP86-D3).[45] A triple-zeta STO basis set TZ2P+[49] was employed in conjunction with the zero-order regular approximation, ZORA,[47] as implemented in ADF2013 software.[50,51] In EDA-NOCV, the interaction energy, ΔE^{int}, is decomposed into physical meaningful terms according to Eq. 1. In EDA-NOCV, ΔE^{elstat} corresponds to the classical electrostatic interactions between the interacting fragments with their frozen charge distribution at the geometry of the complex; ΔE^{Pauli} accounts for the repulsive Pauli interaction between the occupied orbitals of the interacting fragments; and ΔE^{orb} describes not only the interactions between occupied molecular orbitals of one fragment with the unoccupied orbitals of the other fragment (charge transfer), but also the empty/occupied orbital mixing on the same fragment (polarization). Since dispersion corrected functional (BP86-D3) is used, the dispersion correction, ΔE^{disp}, is added to the total interaction energy ΔE^{int}. The EDA-NOCV scheme decomposes the differential density, $\Delta\rho(r)$, into deformation densities, $\Delta\rho_i(r)$, which provides information about the direction of the flow of charge. EDA-NOCV decomposes the orbital component, ΔE^{orb}, into contributions, ΔE_i^{orb}, corresponding to the charge transfer channels, $\Delta\rho_i(r)$. A more detailed description of EDA-NOCV can be found in the origal paper of Mitoraj and coworkers.[32]

$$\Delta E^{int} = \Delta E^{elstat} + \Delta E^{Pauli} + \Delta E^{orb} + \Delta E^{disp} \qquad (1)$$

The topologycal analysis of the anisotropy of the induced current density, ACID, was employed to evaluate the presence of metal-metal and metal-ligand electron delocalisation.[35,36] The ACID calculations were performed by using a internally modified version of the Gaussian03 program.[52] The continuous set of gauge transformation (CSGT)[53–55] was employed to calculate the current densities, by using BP86/def2-TZVPP level of theory. The ACID isosurfaces were plotted at the value of 0.05 and to differentiate the anisotropies of paratropic and diatropic currents, the current density vectors were ploted onto the ACID isosurface. The molecular shielding tensor[56–58] at several points of the molecular domain,[59–61] was calculated within the GIAO formalism, employing the BP86 functional and all-electron Triple-ζ Slater basis set plus two polarization functions (STO-TZ2P) by using the ADF 2012 code.[62,63]

3 Results and Discussion

3.1 Geometries

The optimized structures of complexes **1a-8c** are planar, with dihedral angles (MXNM, X = C, N, or O) equal to zero (Figure S1, supporting information). The calculated structural parameters are in good agreement with the avilable x-ray data.[3,19,25,27,28] For instance, for **1c**, the calculated Au$^+-$N and Au$^+-$Au$^+$ bond distances and the N$-$Au$^+-$N bond angle values are 2.002 Å, 3.360 Å, and 179.7°, the correspondent experimental values are 2.003 Å, 3.387 Å, and 177.0°, respectively. Excelent agreement between calculated and experimental structural parameters is also observed in **3a**, **3c**, **7c**, and **8c** (Figure S1). The atomic radius of gold (174 pm) is larger than that of silver (165 pm) and copper (145 pm).[64] However, the metal-metal bond distances observed in complexes **1a-6c** show clearly the following trend Cu$^+-$Cu$^+$ < Au$^+-$Au$^+$ < Ag$^+-$Ag$^+$, making evident the presence of metalophilicity.[18] In fact, complexes **3b**, **5b**, and **6b** present Ag$^+-$Ag$^+$ bond distances smaller than 3.44 Å, which is the sum of the van der Waals radii of two silver atoms, suggesting the presence of argentophilicity.[65] While the Cu$^+-$Cu$^+$ bond distances of **1a-6c** range from 3.120 Å to 3.295 Å, the Ag$^+-$Ag$^+$ and Au$^+-$Au$^+$ vary from 3.367 Å to 4.094 Å and from 3.271 Å to 3.369 Å, respectively. The results reveal that for copper(I) and gold(I) complexes, the M$-$M distances are slightly dependent on the nature of the ligand employed, while for silver(I) complexes M$-$M distances can change as much as 0.7 Å. The most significant differences are observed on going from **1a-1c** (L = pyrazolate) to **2a-2c** (μ-1,2-isoxazole). In this case, a considerable increase in the M$-$M bond distances is observed. No direct relationship the M$-$M distance and the charge of the ligands, L, is observed (Figure S1). The presence of substituents such as CH_3 and CF_3 in L = pyrazolate (**1c**, **7c**, and **8c**) does not present any significant effect on the M$-$M bond lengths. The calculated M$-$M bond distances for complexes **1c**, **7c**, and **8c** are 3.360 Å, 3.350 Å, and 3.369 Å, respectively, while the correspondent experimental values are 3.387 Å, 3.360 Å, and 3.327 Å, respectively. Likewise the observed trend for metal-ligand, M$-$L, bond distances is Cu$^+-$L < Au$^+-$L < Ag$^+-$L. Such trend does not depend on the nature of the ligand, charge, or coordinating atom (C, N, or O). The observed M$-$L bond distance trend is entirely in line with the results of Wolters and Bickelhaupt,[66] which show a similar trend for simple M$-$L and M$-L_2$ complexes containing M = Cu$^+$, Ag$^+$, Au$^+$ in combination with L = NH_3, PH_3, CO. Comparing the bond distances in **1a-1c** and **2a-2c**, it is observed that M$-$O bond distances are larger than M$-$N, while in complexes **3a-6c** M$-$C bond distances are shorter than M$-$N, independently on the charge of the ligands.

3.2 Bonding Analysis

The EDA-NOCV of **1a**-**8c** was performed by considering $\mathrm{M_3(\mu\text{-}L)_2^{q/q+1}}$ and $\mathrm{L^{0/-}}$, where M = $\mathrm{Au^+}$, $\mathrm{Ag^+}$, $\mathrm{Cu^+}$ and L = pyrazolate with or without substituents R (**1a**-**1c**, **7c**, **8c**), μ-1,2-isoxazole (**2a**-**2c**), μ-2-pyridyl (**3a**-**3c**), μ-pyridazine (**4a**-**4c**), μ-2-pyrimidyl (**5a**-**5c**), and μ-2-pyrazinil (**6a**-**6c**), as interacting fragments (Figure 2). The results reveal that the magnitude of the metal-ligand, M−L, bonding is dependent on the nature of both the ligand and metal employed. In general, a similar trend in the total interaction energy is observed for the same class of complexes. For instance, in complexes containing the pirazolate anion, **1a**-**1c**, $\Delta E^{\mathrm{int}}(\mathrm{Au^+}) < \Delta E^{\mathrm{int}}(\mathrm{Cu^+}) < \Delta E^{\mathrm{int}}(\mathrm{Ag^+})$, indicating that in gold(I) complexes the M−L bonding is stronger than in complexes with copper(I) or silver(I) (Table 1). Such tendency can be understood by the inspection of the physical components in which ΔE^{int} is decomposed. According to Table 1, **1a** presents $\Delta E^{\mathrm{int}} = -235.3\ \mathrm{kcal.mol^{-1}}$, while the values for **1b** and **1c** are $\Delta E^{\mathrm{int}} = -206.2\ \mathrm{kcal.mol^{-1}}$ and $\Delta E^{\mathrm{int}} = -241.0\ \mathrm{kcal.mol^{-1}}$, respectively. The most stable M−L energy interaction of **1c** can be attributed to the largest orbital contribution $\Delta E^{\mathrm{orb}} = -138.4\ \mathrm{kcal.mol^{-1}}$, in comparison with **1a** and **1c**. The results reveals that the M−L interaction in **1c** is mainly electrostatic (73.2%), but with a large covalent character (25.7%) when compared with **1a** (75.6% electrostatic, 23.2% covalent) and **1b** (73.2% electrostatic, 23.3% covalent). The elevated value of $\Delta E^{\mathrm{Pauli}} = 297.2\ \mathrm{kcal.mol^{-1}}$ also confirms the pronounced covalent character of M−L bonds in **1c**. The large covalent character of M−L bonds in **1c** is in agreement with the calculated and experimental bond distances, which show that the $\mathrm{Au^+}$−L bond distances are smaller than $\mathrm{Ag^+}$−L (Figure S1). The NBO analysis (section 3.3) gives support to the elevated covalent character observed for $\mathrm{Au^+}$−L in **1c**, indicating that the ligand-metal donation, L→M, and the metal-ligand back-donation, M→L, are more stabilizing in **1c** than in **1a** or **1b**. The high covalent character in **1c** can be understood in terms of the dominant density deformation channels, $\Delta\rho_1(r)$, and $\Delta\rho_2(r)$, which arises from the ligand-metal donation as shown in Figure S3 (supporting information), providing $\Delta E_1^{\mathrm{orb}} = -45.2\ \mathrm{kcal.mol^{-1}}$ and $\Delta E_2^{\mathrm{orb}} = -42.6\ \mathrm{kcal.mol^{-1}}$ energetic stabilizations. Three other less significant density deformations, $\Delta\rho_3(r)$ - $\Delta\rho_5(r)$, comprises the polarization from the ligand towards the metal centre. Density deformations related with π-back-donation were not observed, which is also in agreement with the results of Wolters and Bickelhaupt,[66] which show the presence of π-back-donation only in bent complexes.

The EDA-NOCV shows that the substitution in a same ligand L, for instance L = pyrazolate ion, has a significant role in the M−L bond strength. On going from **1c** to **7c** and **8c**, the effect of substitution on the $\mathrm{Au^+}$−L bonding energy interaction becomes clear. The presence of $\mathrm{CF_3}$ groups in **7c** destabilize the $\mathrm{Au^+}$−L bonding interaction energy from $\Delta E^{\mathrm{int}} = -241.0\ \mathrm{kcal.mol^{-1}}$, **1c**, to $\Delta E^{\mathrm{int}} = -227.3\ \mathrm{kcal.mol^{-1}}$, **7c** (Table 1). The replacement of hydrogen atoms in **1c** by $\mathrm{CF_3}$ and $\mathrm{CH_3}$ groups in tandem, **8c**, causes to the $\mathrm{Au^+}$−L bond a moderate weakening, $\Delta E^{\mathrm{int}} = -233.3\ \mathrm{kcal.mol^{-1}}$. The substitution affects the strength of the $\mathrm{Au^+}$−L bond, but does not change its nature. According to Table 1, the electrostatic (70.6 - 73.2%) and orbital (25.7 - 27.4%) contributions to the $\mathrm{Au^+}$−L bonding in **1c**, **7c**, and **8c** remain similar.

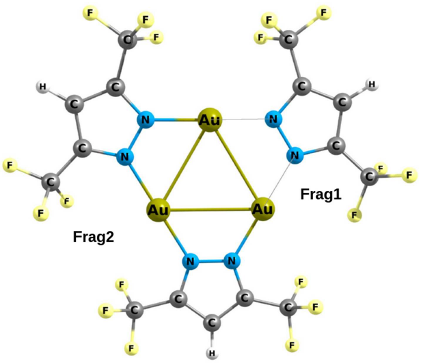

Fig. 2 Fragmentation scheme adopted in EDA-NOCV of Complexes **1a**-**8c**. As an example, $[\mathrm{(CF_3)_2Pz}]^-$ (**Frag1**) and $[\mathrm{(Au)_3(\mu\text{-}3,5\text{-}(CF_3)Pz)_2}]^+$ (**Frag2**) are considered as interacting fragments of complex **7c**.

The bonding scheme in CTC involves the charge transfer from the respective donor ligand towards the coinage $\mathrm{M_3^{3+}}$ core (M = Cu, Ag, Au). The resulting covalent interaction leads to the population of the initially unocupied ns shells (n = 3, 4, or 5, for Cu, Ag, and Au respectively), which under the D_{3h} point group their combination span as $\Gamma^{ns}_{D3h} = a_1' \oplus e_1'$, which describes a highly bonding and slightly antibonding combinations within the $\mathrm{M_3^{3+}}$ core, respectively. The analysis of selected systems, Table 2, reveals that in the pyrazolate derivatives (**1a**-**1c**) the population of the totally symmetric ns combination (a_1') and the two-fold antibonding combination (e_1') increases in the order (Figure 3), **1b** < **1a** < **1c**, in agreement to the interaction energy (ΔE^{int}) discussed above. The populations of both bonding and slightly antibonding ns combinations are in similar amount, which accounts for the long $\mathrm{d^{10}}$−$\mathrm{d^{10}}$ contact supported mainly by the ligand-metal and metallophilic interactions. Such situation neglect the possibility of an effective bonding situation within the core as has been characterized for short $\mathrm{d^{10}}$−$\mathrm{d^{10}}$ cases,[23] where the $\mathrm{d^{10}}$−$\mathrm{d^{10}}$ distance is considerable lesser than the sum of their van der waals radii as has been depicted for example in the pentameric $[\mathrm{Au_5(Mes)_5}]$ compound with Au-Au of about 2.8 Å.[23] Thus, in the case of **1a**, **1b** and **1c**, the population of the different

Table 1 Energy decomposition analysis, EDA-NOCV (kcal.mol^{-1}), for complexes **1a**-**8c**, by considering $M_3(\mu\text{-L})_2^{q/q+1}$ and $L^{0/-}$ as interacting fragments (Figure S1, suporting information), employing BP86-D3/TZ2P+ as level of theory.

CTC	ΔE^{int}	ΔE^{Pauli}	ΔE^{elstat}	ΔE^{orb}_{tot}	ΔE^{orb}_{1}	ΔE^{orb}_{2}	ΔE^{orb}_{3}	ΔE^{orb}_{4}	ΔE^{orb}_{5}	ΔE^{orb}_{res}	ΔE^{disp}
1a	-235.3	189.7	-321.2	-98.5	-30.2	-22.7	-11.1	-5.6	-4.3	-24.6	-5.3
			(75.6%)	(23.2%)							(1.2%)
1b	-206.2	153.4	-270.8	-83.8	-28.1	-22.8	-7.3	-3.9	-3.7	-18.0	-5.0
			(75.3%)	(23.3%)							(1.4%)
1c	-241.0	297.2	-393.7	-138.4	-45.2	-42.6	-11.9	-5.4	-5.3	-28.0	-6.0
			(73.2%)	(25.7%)							(1.1%)
7c	-227.3	275.1	-354.7	-137.5	-42.3	-40.4	-14.1	-6.4	-5.3	-29.0	-10.2
			(70.6%)	(27.4%)							(2.0%)
8c	-233.3	285.2	-370.1	-139.1	-44.0	-41.0	-13.0	-5.7	-5.1	-30.3	-9.3
			(71.4%)	(26.8%)							(1.8%)
2a	-117.8	104.5	-127.3	-90.3	-26.4	-15.9	-16.0	-5.9	-5.8	-20.3	-4.8
			(57.2%)	(40.6%)							(2.1%)
2b	-77.6	57.8	-77.1	-53.9	-19.5	-8.8	-9.1	-3.6	-2.9	-10.0	-4.4
			(56.9%)	(39.8%)							(3.2%)
2c	-118.7	190.1	-178.4	-124.1	-50.4	-20.5	-17.8	-9.6	-6.8	-19.0	-6.3
			(57.8%)	(40.2%)							(2.0%)
3a	-242.5	249.8	-379.4	-107.1	-36.4	-25.5	-9.6	-6.2	-5.9	-23.5	-5.9
			(77.1%)	(21.8%)							(1.1%)
3b	-216.2	220.0	-337.1	-94.0	-37.2	-23.3	-5.9	-5.1	-4.3	-18.2	-5.1
			(77.3%)	(21.5%)							(1.1%)
3c	-252.3	438.1	-529.8	-154.3	-65.0	-37.0	-11.7	-9.8	-5.9	-24.9	-6.2
			(76.7%)	(22.4%)							(0.9%)
4a	-150.4	139.3	-181.3	-102.4	-26.7	-17.7	-24.4	-9.4	-4.2	-20.0	-6.0
			(62.6%)	(35.3%)							(2.1%)
4b	-113.7	95.4	-128.7	-75.2	-20.9	-21.1	-11.2	-6.5	-2.8	-12.7	-5.2
			(61.5%)	(36.0%)							(2.5%)
4c	-156.8	227.3	-239.4	-138.3	-41.4	-40.2	-18.7	-9.9	-5.4	-22.7	-6.3
			(62.3%)	(36.0%)							(1.6%)
5a	-240.3	251.5	-377.1	-109.4	-41.5	-24.4	-9.2	-6.8	-6.0	-21.5	-5.3
			(76.7%)	(22.2%)							(1.0%)
5b	-212.5	218.1	-328.7	-96.9	-43.8	-21.6	-5.6	-4.9	-4.4	-16.6	-5.0
			(76.3%)	(22.5%)							(1.1%)
5c	-250.0	438.4	-524.5	-157.9	-70.7	-35.8	-11.9	-10.1	-6.2	-23.2	-5.9
			(76.2%)	(22.9%)							(0.9%)
6a	-243.5	250.2	-379.7	-108.4	-38.8	-25.2	-9.9	-6.4	-6.1	-22.0	-5.7
			(76.8%)	(22.0%)							(1.1%)
6b	-216.2	216.3	-334.0	-93.6	-37.9	-23.0	-6.2	-4.2	-5.1	-17.2	-5.0
			(77.2%)	(21.6%)							(1.1%)
6c	-252.4	438.1	-527.4	-157.0	-68.6	-37.1	-12.0	-10.3	-6.1	-22.9	-6.1
			(76.4%)	(22.7%)							(0.9%)

Table 2 Population of the ns combination of the M_3^{3+} core in selected systems.

CTC	a_1'	e_1'	CTC	a_1'	e_1'
1a	0.89	1.25	**2c**	0.93	1.19
1b	0.75	1.16	**3c**	0.70	1.16
1c	1.04	1.71	**4c**	0.92	1.28
			5c	0.80	1.48
			6c	0.77	1.22

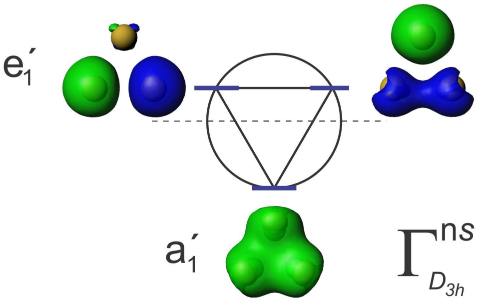

Fig. 3 Frost diagram to the denote qualitatively the bonding and antibonding character of the ns combination for the M_3^{3+} core.

combinations derived from each ns atomic orbital denotes a rather small bonding interaction within the M_3^{3+} core. The evaluation of golden counterpart for **2**, **3**, **4**, **5**, and **6** denotes the variation of the population of the ns based levels according to the respective stabilizing ligand.

In CTCs chemistry, pyrazolate is the most common bridging ligand, while the occurence of CTCs containing isoxazole or isothiazole as bridging ligands is not reported in the literature so far. By comparing EDA-NOCV results for **1a**-**1c** and **2a**-**2c** (Table 1), it is observed that the M−L bonding interaction energies are destabilized on going from **1a** to **2a**. While **1a** shows $\Delta E^{int} = -321.2$ kcal.mol^{-1}, the correspondent values for **2a** is $\Delta E^{int} = -127.3$ kcal.mol^{-1}. Similarly, on going form **1b** to **2b** and from **1c** to **2c**, the ΔE^{int} values range from -206.2 kcal.mol^{-1} to -77.6 kcal.mol^{-1} and from -241.0 kcal.mol^{-1} to -118.7 kcal.mol^{-1}, respectively. The destabilization in the total bonding energies of **2a**-**2c** in comparison with **1a**-**1c** stems from the decrease of both electrostatic and orbital stabilization in M−L bonds, particularly because pyrazolate is an anion, while isoxazole is neutral ligand. The smaller orbital stabilization in **2a**-**2c** emerges from the presence of oxygen atom in isoxazole ligands, which is harder than nitrogen, in agreement with the Pearsons principle of hard and soft acids and bases (HSAB).[67] The differences in the ΔE^{int} between **2a**-**2c** and **1a**-**1c** are consistent with the Pearsons principle. According to EDA-NOCV, negatively charged ligands (**1a**-**1c**, **7c**-**1c**, **3a**-**3c**, **5a**-**6c**) coordinate strongly in comparison with neutral ligands, (**2a**-**2c** and **4a**-**4c**) independently of the nature of the ligand, or ring size (Table 1, Figure 1). For instance in complexes **3a**-**3c**, in which L = μ-2-pyridyl anion, an heterocyclic six-membered ring, the bonding interactions are stronger than in complexes **4a**-**4c**, where L = μ-pyridazine is employed. The relative position of heteroatoms in μ-2-pyrimidyl (**5a**-**5c**) and μ-2-pyrazinil (**6a**-**6c**) does not present any significant effect on the strength of the M−L bonding interaction energies.

3.3 NBO analysis

The bond orders and NPA charges indicate that the metal-ligand interactions in complexes **1a**-**8c** are closed-shell interactions. The largest bond orders were observed for gold(I) complexes (Table S1). The Cu−N, Ag−N, and Au−N bond order values in **1a**, **1b**, and **1c** are 0.298, 0.340, and 0.455, respectively. It is also in agreement with the natural charges, which indicate that more amount of charge is transfered from N to Au^+, in comparison with Cu^+ and Ag^+ (Table S1). The NBO analysis does not reveal the presence of metal-metal interactions in **1a**-**1c**. The M−M bond order values are negligible. The presence of substituents like CH_3 and CF_3 in the pyrazolate ring, **7c** and **8c**, just has a very small effect on the bond orders and atomic charges (Table S1), indicating that the electron-withdrawing groups, CF_3, cause a small decrease on the Au−N bond orders, while electron-donor groups, CH_3, when employed in conjunction with CF_3 tend to compensate such effect, yielding slightly increased Au−N bond orders in comparison with **1c**. All complexes **2a**-**6c** exhibit similar trends as **1a**-**1c** in terms of bond orders and atomic charges. For instance, for **2a**-**2c** and **4a**-**4c**, the largest metal-ligand bond order values are observed for complexes containing Au^+, while complexes with Cu^+ and Ag^+ present similar bond orders (Table S1). The ligand→metal charge transfer is also more pronounced in complexes containing Au^+ (Table S1). These results are in agreement with EDA-NOCV (Table S1), making evident that in gold(I) complexes the M-L bonding is stronger than in complexes with copper(I) or silver(I).

The second-order stabilization energies, ΔE^2, obtained with NBO method[34] for some selected complexes, **1a**-**1c**, **2a**-**2c**, **4a**-**4c**, and **7c**-**8c**, confirm that L→M donations are much more stronger than M→L back-donation (Table S2), in line with EDA-NOCV results NBO analysis shows that the L→M bonding in **1a**-**1c** results from the overlap of a hybrid lonepair $n_{sp^{2.73}}$ on N with the antibonding orbital σ^* on M−N bonding, providing stabilizations that range from 59.1 to 137.7 kcal.mol^{-1}. As observed in Table S2, the strongest stabilization for L→M donations are observed for gold(I) complexes, **1c**, **7c**, and **8c**. The effect of substituents CH_3 and CF_3 are in agreement with the EDA-NOCV results, indicating that presence of CF_3 groups in **7c** destabilizes the Au^+−L bonding, while the concomitant presence of CH_3 minimize this effect. On the other hand, the M→L back-bonding is not significant, providing stabilizations that range from 0.98 to 4.32 kcal.mol^{-1}. As observed in the EDA-NOCV analysis, the NBO results also confirm the metal-ligand bond destabilization on going from pyrazolate ligand, **1a**-**1c**, to isoxazole, **2a**-**2c** (Table S2). According to NBO analysis the L→M interactions in **2a**-**2c** provide stabilizations varying from 11.9 to 45.4 kcal.mol^{-1}. These findinds combined with EDA-NOCV results reveal that CTCs containing isoxazole are less stable than those containing pyrazolate, indicanting that the strenght of L→M donations is dependent on the nature of both the coinage metal and the ligand employed. For instance, when μ-pyridazine is employed, **4a**-**4c**, the L→M donations and M→L back-donations magnitudes differ significantly in comparison with **1a**-**1c** or **2a**-**2c** (Table S2, Figure 4).

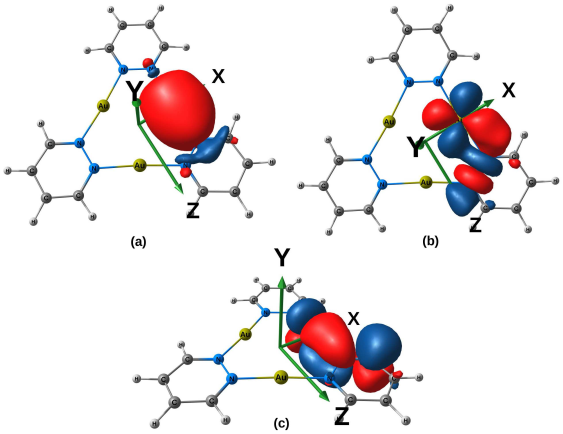

Fig. 4 Schematic representation of (a) $\mathrm{n}_{sp^{2.02}}(\mathrm{N}) \rightarrow s(\mathrm{Au})$, (b) $\mathrm{d}_{xz}(\mathrm{Au}) \rightarrow \sigma^{*}(\mathrm{N{-}N})$, and (c) $\mathrm{d}_{yz}(\mathrm{Au}) \rightarrow \pi^{*}(\mathrm{N{-}C})$ NBO interactions in **4c**.

3.4 Anisotropy of the Induced Current Density (ACID) and Magnetic Response

Since EDA-NOCV and NBO analyses do not provided significant evidence of metal-metal interactions or *through-space* conjugation between the metalic centers, the anisotropy of the induced current density (ACID) and the magnetic response properties were evaluated in order to shed some light on this point. The ACID method provides a spatial representation of the delocalized electrons, making possible to quantify and to visualize different types of conjugative effects and aromaticity.[35,36]

The ACID plots, as a clockwise and counterclockwise circulation, respectively, for some selected complexes is presented in Figure 5. The ACID plots for all complexes is presented in Figure S2. According to ACID (Figure 5), the pyrazolate ligands (**1a**-**1c**) exhibit a very high degree of conjugation, in agreement with the magnetic response (below). There is cyclic conjugation in these ligands and according to the current density vectors, a strong diatropic ring current indicating the presence of aromaticity. However, there is no *through-bond* M−L conjugation between the ligands and the metalic centers, as indicated by the absence of a continuous boundary surface involving M−L. Despite the fact that in some systems like **1c** and **2c** present pronounced anisotropy towards the metalic centers, the presence zero-flux surface is still observed. According to ACID, no conjugation between the metalic centers is oberved. Substituted derivatives of **1c**, **7c** and **8c**, the presence and the absence of hyperconjugative stabilizations from CH_3 and CF_3 substituents are observed. ACID isosurfaces in the M_3^{3+} cores are slightly large for gold(I), than for copper(I) or silver(I).

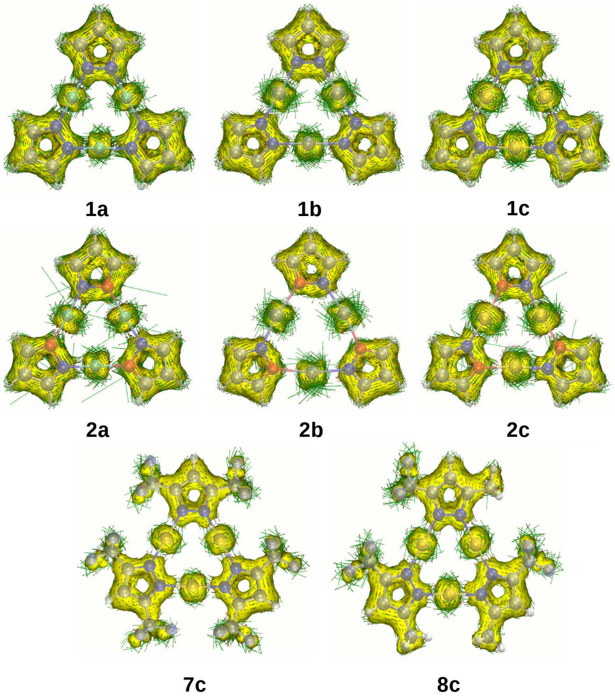

Fig. 5 ACID plots of complexes **1a**-**1c**, **2a**-**2c**, **7c**, and **8c** at 0.05 isosurface.

Magnetic response properties provide a powerful tool for studying the chemical environment of the individual nucleus produced by its neighbors and the nucleus itself.[56–58] Besides the magnetic response given by a probe nucleus in NMR experiments, the response of the molecule can be conveniently generalized through the space, allowing to account for short- and long-range magnetic behavior driven by induced currents.[59–61] In this concern, the evaluation of the magnetic behavior of selected systems which exhibits long $d^{10}{-}d^{10}$ intramolecular interaction is described in terms of the secondranked magnetic shielding tensor σ_{ij}[56–61] for a given point in the space, which relates the molecular response (B^{ind}) to a uniform external magnetic field (B^{ext}), as follows, $B^{ind} = -\sigma_{ij}B^{ext}_j$. With the aim to rationalize this *through-space* quantity in terms to shielding or deshielding shift in NMR experiments,[57,58] we consider the relationship between each component of the magnetic shielding (σ_{ij}) and chemical shift (δ_{ij}) tensors, given by $\delta = (\sigma_{ref} - \sigma)/(1-\sigma) \approx (\sigma_{ref} - \sigma)$, where σ^{ref} is equal to zero for a given nucleus-independent point in the space, leading to the following relationship for each component of such tensor:[57,58] $\delta_{ij} = -\sigma_{ij}$.

The representation of δ_{ij} into the space allows to obtain a visualization of the shielding (negative values of δ_{ij}) and deshielding regions (positive values of δ_{ij}),[59–61] which, in turn denotes the presence of diatropic or paratropic induced currents in the space.[57,58] It is well-known that the magnetic properties are influenced by the relativistic effects denoted by σ[68–71] and therefore affect the evaluation of δ as described through the vicinal heavy-atom effect on light atoms (HALA effect) and by the effects on the shielding of the heavy atom itself (HAHA effect).[72–75] Hence, our calculation includes both scalar and spin–orbit effects with the aim to take into account the relativistic effects.[68]

For the description of the tensor quantities derived from a nucleus-independent point in the molecular space, we define our frame of reference in relation to a molecule-fixed Cartesian coordinate system (x, y, z) where the z-axis is perpendicular to the plane defined by the M_3^{3+} core. In order to account for the local and remote effects,[56] at the nucleus and the neighbour anisotropic contributions to the magnetic response, respectively, by producing the observed shielding, we consider the fast tumbling of the molecule in solution, which average the components of δ_{ij} leading to the isotropic component, $\delta_{iso} = \frac{1}{3}(\delta_{xx} + \delta_{yy} + \delta_{zz})$ (Figure 6).[56–58] The δ_{iso} for **1a**, **1b** and **1c** (Figure 6), describes the slight interaction between the closed-shell centers due that the remote effect (or anisotropic effect) caused by each nucleus does not influence considerably the neighbor center.[21] This result agrees with the analysis of the population of the ns (Γ^{ns}) derived levels within the M_3^{3+} core, leading to long $d^{10}-d^{10}$ contacts. At the center of the ring the δ_{iso} values (also denoted as NICS(0)) denotes values of about -1.5 ppm along the pyrazolate series, whereas the value at the center of the M^+-M^+ distance increases slightly as, -1.5 ppm (**1a**) < -1.7 ppm (**1b**) < -3.6 ppm (**1c**). Going down in the XI group, the isotropic magnetic response describes a similar behavior for the pyrazolate moieties.

From the zz-component (δ_{zz}), the complexity of the magnetic response is denoted which exhibits larger differences between **1a**, **1b** and **1c**, where paratropic response (positive values) increases within the metallic core in relation to the number of inner electrons.[37] Throughout the series the pyrazolate moieties exhibits the characteristic magnetic response for aromatic 6π rings with diatropic currents at the center of the ligand and paratropic currents outside the ring, which are more pronounced towards the M_3^{3+} core. The golden counterpart **1c** exhibits the larger magneto-responsive behavior,[76] which is clearly denoted by the analysis of certain components of δ, δ_{zz} in our case. The aromatic character of organic and inorganic rings has been widely related to the magnetic response in the space at certain points in the ring and also to the contribution from the frontier orbitals.[77] However, according to the increase of the atomic number of the involved nucleus, the through-the-space magnetic response is highly influenced by the contribution from the inner electrons, which particularly take part into the diamagnetic term derived from the Ramsey theory of the magnetic shielding for nucleus in molecules,[37,78] which involves solely the groundstate wavefunction of the system. Thus the analysis of the aromatic behavior from the magnetic criteria in heavy elements systems should be complemented by other molecular properties. In **1a**, **1b**, and **1c**, the rather small bonding interaction within the M_3^{3+} core suggest a non-aromatic behavior, in agreement with the ACID analysis, reported above (Figure 5), the magnetic criteria seems to be not enough to determinate the aromatic character for heavy atoms systems). The comparison with selected ligands (Figure 7) namely, 1,2-isoxazole (**2c**), 2-pyridil (**3c**) and pyridazine (**4c**) describes an overall magnetic behavior related to **1c**, with slight differences. At the center of the ring, the nucleus independent probe denote isotropic values of 1.48 ppm for **3c**, 1.53 ppm for **1c**, 2.22 ppm for **4c** and 4.17 ppm for **2c**.

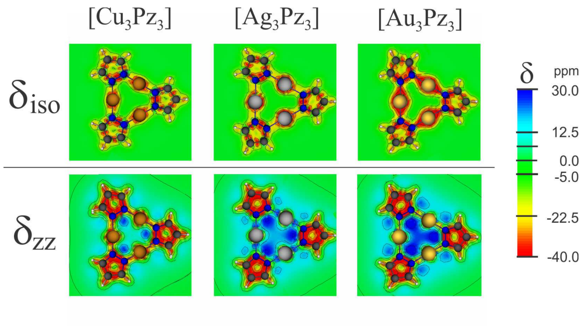

Fig. 6 Chemical shift map over the molecular domain, denoting the δ_{iso} and δ_{zz} components, for [Cu_3Pz_3], [Ag_3Pz_3] and [Au_3Pz_3].

4 Conclusions

The geometrical parameters such metal-metal bond distances of optimized structures of complexes **1a-6c** show clearly the following trend $Cu^+-Cu^+ < Au^+-Au^+ < Ag^+-Ag^+$, making evident the presence of metalophilic interactions. The M−M distances are slightly dependent on the nature of the ligand. The metal-ligand, M−L, bond distances presented the

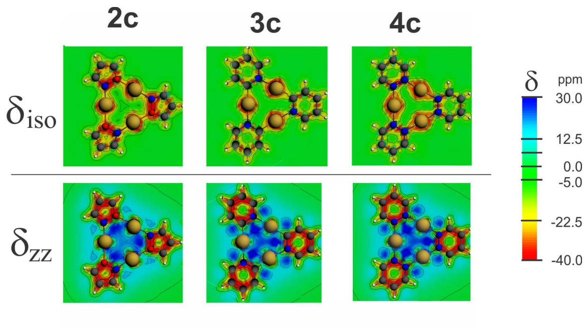

Fig. 7 Chemical shift map over the molecular domain, denoting the δ_{iso} and δ_{zz} components, for **2c**, **3c** and **4c**.

following trend Cu^{+}–L $<$ Au^{+}–L $<$ Ag^{+}–L, which is independent on the nature of the ligand, charge, or coordinating atom (C, N, or O). The EDA-NOCV results show that the magnitude of the metal-ligand, M–L, bonding is dependent on the nature of both the ligand and coinage metal employed. Particularly, the EDA-NOCV reveals that the M–L bonding is stronger in gold(I) than in copper(I) or silver(I) complexes and that Au^{+}–L bonds present a elevated covalent character when compared with Cu^{+}–L and Ag^{+}–L bonds, in agreement with Wolters and Bickelhaupt.[66] The NBO analysis confirms this elevated covalent character, indicating that the ligand-metal donation, L$\rightarrow$M, and the metal-ligand back-donation, M$\rightarrow$L, are more stabilizing in gold(I) than in copper(I) or silver(I) complexes. The obtained results describe that the ligand σ-donation is the main bonding scheme stabilizing the M$_3^{3+}$ core, which is slightly contributed by a π-backdonation. The populations of both bonding and slightly antibonding ns orbital combinations are in similar amount, which accounts for the long d^{10}–d^{10} contact supported mainly by the ligand-metal and metallophilic interactions. In the case of **1a**, **1b** and **1c**, the population of the different combinations derived from each ns atomic orbital denotes a rather small bonding interaction within the M$_3^{3+}$ core. Both ACID and the magnetic response calculations show that there is cyclic conjugations in the ligands and a strong diatropic ring current indicating the presence of aromaticity. However, there is no *through-bond* M–L conjugation between the ligands and the metalic centers in CTCs, as indicated by the absence of a continuous anisotropy boundary surface involving M–L bonds.

5 Acknowledgement

The authors thank the National Council for Scientific and Technological Development (CNPq) for the financial support (grant 470985/2011-9) and the excellent service of the Hochschulrechenzentrum of the Philipps-Universitt Marburg. GFC thanks the Capes (Coordination for the Improvement of Higher Level -or Education- Personnel) for the post-doc research scholarship (grant 3181-13-8). DMA thanks the Deutscher Akademischer Austauschdienst for a postdoctoral scholarship. A.M.-C. thanks to Fondecyt 1140359.

References

1 M. A. Omary, M. A. Rawashdeh-Omary, M. W. A. Gonser, O. Elbjeirami, T. Grimes, T. R. Cundari, H. V. K. Diyabalanage, C. S. P. Gamage and H. V. R. Dias, *Inorg. Chem.*, 2005, **44**, 8200–8210.
2 L. Hou, W.-J. Shi, Y.-Y. Wang, H.-H. Wang, L. Cui, P.-X. Chen and Q.-Z. Shi, *Inorg. Chem.*, 2011, **50**, 261–270.
3 A. Burini, A. A. Mohamed and J. P. Fackler, *Comm. Inorg. Chem.*, 2003, **24**, 253–280.
4 A. A. Mohamed, J. M. Lòpez-de Luzuriaga and J. P. J. Fackler, *J. Clust. Sci.*, 2003, **14**, 61–70.
5 A. A. Mohamed, A. Burini and J. P. Fackler, *J. Am. Chem. Soc.*, 2005, **127**, 5012–5013.
6 A. A. Mohamed, R. Galassi, F. Papa, A. Burini and J. P. Fackler, *Inorg. Chem.*, 2006, **45**, 7770–7776.
7 A. A. Mohamed, L. M. Prez and J. P. Fackler Jr., *Inorg. Chim. Acta*, 2005, **358**, 1657–1662.
8 M. A. Omary, A. A. Mohamed, M. A. Rawashdeh-Omary and J. P. Fackler Jr., *Coord. Chem. Rev.*, 2005, **249**, 1372–1381.
9 H. V. R. Dias and C. Palehepitiya Gamage, *Angew. Chem. Int. Ed.*, 2007, **46**, 2192–2194.
10 H. V. R. Dias, S. Singh and C. F. Campana, *Inorg. Chem.*, 2008, **47**, 3943–3945.
11 J.-P. Zhang and S. Kitagawa, *J. Am. Chem. Soc.*, 2008, **130**, 907–917.
12 S. M. Tekarli, T. R. Cundari and M. A. Omary, *J. Am. Chem. Soc.*, 2008, **130**, 1669–1675.
13 H. V. R. Dias, C. S. P. Gamage, J. Keltner, H. V. K. Diyabalanage, I. Omari, Y. Eyobo, N. R. Dias, N. Roehr, L. McKinney and T. Poth, *Inorg. Chem.*, 2007, **46**, 2979–2987.
14 A. A. Titov, O. A. Filippov, A. N. Bilyachenko, A. F. Smol'yakov, F. M. Dolgushin, V. K. Belsky, I. A. Godovikov, L. M. Epstein and E. S. Shubina, *Eur. J. Inorg. Chem.*, 2012, **2012**, 5554–5561.
15 G. Yang, P. Baran, A. R. Martnez and R. G. Raptis, *Crystal Growth & Design*, 2013, **13**, 264–269.
16 S.-Z. Zhan, M. Li, S. W. Ng and D. Li, *Chem. Eur. J.*, 2013, **19**, 10217–10225.
17 L. G. Vaughan, *J. Am. Chem. Soc.*, 1970, **92**, 730–731.
18 P. Pyykkö, *Chem. Rev.*, 1988, **88**, 563–594.
19 G. Yang and R. G. Raptis, *Inorg. Chem.*, 2003, **42**, 261–263.
20 H. Schmidbaur, *Gold Bull*, 2000, **33**, 3–10.
21 R. G. Maturana, M. P. Vargas and A. Muñoz–Castro, *J. Phys. Chem. A*, 2012, **116**, 8737–8743.
22 A. Muñoz–Castro and R. G. Maturana, *J. Phys. Chem. C*, 2014, **118**, 21185–21191.
23 A. Muñoz–Castro, *Phys. Chem. Chem. Phys.*, 2014, **16**, 7578–7583.
24 M. A. Halcrow, *Dalton Trans.*, 2009, 2059–2073.
25 B. Bovio, F. Bonati and G. Banditelli, *Inorg. Chim. Acta*, 1984, **87**, 25–33.
26 P. Ovejero, M. J. Mayoral, M. Cano and M. C. Lagunas, *J. Organomet. Chem.*, 2007, **692**, 1690–1697.
27 M. W. Dodge, W. F. Wacholtz and J. T. Mague, *J Chem Crystallogr*, 2005, **35**, 5–12.
28 F. García, A. D. Hopkins, R. A. Kowenicki, M. McPartlin, M. C. Rogers and D. S. Wright, *Organometallics*, 2004, **23**, 3884–3890.
29 H. H. Murray, R. G. Raptis and J. P. Fackler, *Inorg. Chem.*, 1988, **27**, 26–33.
30 R. G. Raptis and J. P. Fackler, *Inorg. Chem.*, 1988, **27**, 4179–4182.

31 A. A. Titov, O. A. Filippov, E. A. Guseva, A. F. Smol'yakov, F. M. Dolgushin, L. M. Epstein, V. K. Belsky and E. S. Shubina, *RSC Adv.*, 2014, **4**, 8350–8359.

32 M. P. Mitoraj, A. Michalak and T. Ziegler, *J. Chem. Theory Comput.*, 2009, **5**, 962–975.

33 E. D. Glendening, C. R. Landis and F. Weinhold, *WIREs: Comput. Mol. Sci.*, 2012, **2**, 1–42.

34 A. E. Reed, L. A. Curtiss and F. Weinhold, *Chem. Rev.*, 1988, **88**, 899–926.

35 D. Geuenich, K. Hess, F. Köhler and R. Herges, *Chem. Rev.*, 2005, **105**, 3758–3772.

36 R. Herges and D. Geuenich, *J. Phys. Chem. A*, 2001, **105**, 3214–3220.

37 A. Muñoz–Castro, *J. Phys. Chem. C*, 2012, **116**, 17197–17203.

38 A. Muñoz–Castro, *J. Phys. Chem. A*, 2011, **115**, 10789–10794.

39 P. Hohenberg and W. Kohn, *Phys. Rev.*, 1964, **136**, B864–B871.

40 W. Kohn and L. J. Sham, *Phys. Rev.*, 1965, **140**, A1133–A1138.

41 A. D. Becke, *Phys. Rev. A*, 1988, **38**, 3098–3100.

42 J. P. Perdew, *Phys. Rev. B*, 1986, **33**, 8822–8824.

43 S. Grimme, *J. Comput. Chem.*, 2006, **27**, 1787–1799.

44 S. Grimme, S. Ehrlich and L. Goerigk, *J. Comput. Chem.*, 2011, **32**, 1456–1465.

45 S. Grimme, J. Antony, S. Ehrlich and H. Krieg, *J. Chem. Phys.*, 2010, **132**, 154104.

46 F. Weigend and R. Ahlrichs, *Phys. Chem. Chem. Phys.*, 2005, **7**, 3297–3305.

47 E. van Lenthe, E. J. Baerends and J. G. Snijders, *J. Chem. Phys.*, 1993, **99**, 4597–4610.

48 F. Neese, *WIREs: Comp. Mol. Sci.*, 2012, **2**, 73–78.

49 E. Van Lenthe and E. J. Baerends, *J. Comput. Chem.*, 2003, **24**, 11421156.

50 G. te Velde, F. M. Bickelhaupt, E. J. Baerends, C. Fonseca Guerra, S. J. A. van Gisbergen, J. G. Snijders and T. Ziegler, *J. Comput. Chem.*, 2001, **22**, 931967.

51 C. F. Guerra, J. G. Snijders, G. t. Velde and E. J. Baerends, *Theor. Chem. Acc.*, 1998, **99**, 391–403.

52 M. J. Frisch, G. W. Trucks, H. B. Schlegel, G. E. Scuseria, M. A. Robb, J. R. Cheeseman, J. A. Montgomery, Jr., T. Vreven, K. N. Kudin, J. C. Burant, J. M. Millam, S. S. Iyengar, J. Tomasi, V. Barone, B. Mennucci, M. Cossi, G. Scalmani, N. Rega, G. A. Petersson, H. Nakatsuji, M. Hada, M. Ehara, K. Toyota, R. Fukuda, J. Hasegawa, M. Ishida, T. Nakajima, Y. Honda, O. Kitao, H. Nakai, M. Klene, X. Li, J. E. Knox, H. P. Hratchian, J. B. Cross, V. Bakken, C. Adamo, J. Jaramillo, R. Gomperts, R. E. Stratmann, O. Yazyev, A. J. Austin, R. Cammi, C. Pomelli, J. W. Ochterski, P. Y. Ayala, K. Morokuma, G. A. Voth, P. Salvador, J. J. Dannenberg, V. G. Zakrzewski, S. Dapprich, A. D. Daniels, M. C. Strain, O. Farkas, D. K. Malick, A. D. Rabuck, K. Raghavachari, J. B. Foresman, J. V. Ortiz, Q. Cui, A. G. Baboul, S. Clifford, J. Cioslowski, B. B. Stefanov, G. Liu, A. Liashenko, P. Piskorz, I. Komaromi, R. L. Martin, D. J. Fox, T. Keith, M. A. Al-Laham, C. Y. Peng, A. Nanayakkara, M. Challacombe, P. M. W. Gill, B. Johnson, W. Chen, M. W. Wong, C. Gonzalez and J. A. Pople, *Gaussian 03, Revision D.01*, Gaussian, Inc., Wallingford, CT, 2004.

53 T. A. Keith and R. F. W. Bader, *Chem. Phys. Lett.*, 1992, **194**, 1–8.

54 T. A. Keith and R. F. W. Bader, *J. Chem. Phys.*, 1993, **99**, 3669–3682.

55 J. R. Cheeseman, G. W. Trucks, T. A. Keith and M. J. Frisch, *J. Chem. Phys.*, 1996, **104**, 5497–5509.

56 R. S. Drago, *Physical Methods in Chemistry*, W.B. Saunders: Philadelphia, PA., 1977, p. chapter VII.

57 M. Kaupp, M. Bühl and V. G. Malkin, *Calculation of NMR and EPR Parameters. Theory and Applications*, Wiley-VCH Verlag GmbH & Co. KGaA, Weinheim, Germany, 2004.

58 T. Heine, C. Corminboeuf and G. Seifert, *Chem. Rev.*, 2005, **105**, 3889–3910.

59 S. Klod and E. Kleinpeter, *J. Chem. Soc., Perkin Trans. 2*, 2001, 1893–1898.

60 J. Aihara and S. Oe, *Bull. Chem. Soc. Jpn.*, 2003, **76**, 1363–1364.

61 D. Sebastiani, *ChemPhysChem*, 2006, **7**, 164–175.

62 G. te Velde, F. M. Bickelhaupt, E. J. Baerends, C. Fonseca Guerra, S. J. A. van Gisbergen, J. G. Snijders and T. Ziegler, *J. Comput. Chem.*, 2001, **22**, 931–967.

63 C. F. Guerra, J. G. Snijders, G. te Velde and E. J. Baerends, *Theor. Chem. Acc.*, 1998, **99**, 391–403.

64 E. Clementi and D. L. Raimondi, *J. Chem. Phys.*, 1963, **38**, 2686–2689.

65 L. Koskinen, S. Jskelinen, L. Oresmaa and M. Haukka, *Cryst. Eng. Comm.*, 2012, **14**, 3509–3514.

66 L. P. Wolters and F. M. Bickelhaupt, *ChemistryOpen*, 2013, **2**, 106–114.

67 R. G. Pearson, *J. Am. Chem. Soc.*, 1963, **85**, 3533–3539.

68 K. G. Dyall and K. Faegri, *Introduction to Relativistic Quantum Chemistry*, Oxford University Press, New York, 2007.

69 N. C. Pyper and Z. C. Zhang, *Mol. Phys.*, 1999, **97**, 391–413.

70 N. C. Pyper, *Chem. Phys. Lett.*, 1983, **96**, 204–210.

71 G. Schreckenbach and T. Ziegler, *Theor. Chem. Acc.*, 1998, **99**, 71–82.

72 U. Edlund, T. Lejon, P. Pyykkö, T. K. Venkatachalam and E. Buncel, *J. Am. Chem. Soc.*, 1987, **109**, 5982–5985.

73 P. Pyykkö, A. Görling and N. Rösch, *Mol. Phys.*, 1987, **61**, 195–205.

74 M. Kaupp, O. L. Malkina, V. G. Malkin and P. Pyykkö, *Chem. Eur. J.*, 1998, **4**, 118–126.

75 P. Lantto, R. H. Romero, S. S. Gómez, G. A. Aucar and J. Vaara, *J. Chem. Phys.*, 2006, **125**, 184113.

76 E. E. Karagiannis and C. A. Tsipis, *Organometallics*, 2010, **29**, 847–859.

77 N. D. Charistos, A. G. Papadopoulos and M. P. Sigalas, *J. Phys. Chem. A*, 2014, **118**, 1113–1122.

78 N. F. Ramsey, *Phys. Rev.*, 1950, **78**, 699–703.